Article

Equivalent Temperature-Enthalpy Diagram for the Study of Ejector Refrigeration Systems

Mohammed Khennich, Mikhail Sorin * and Nicolas Galanis

Department of Mechanical Engineering, Université de Sherbrooke, Sherbrooke, QC J1K2R1, Canada;
E-Mails: Mohammed.Khennich@USherbrooke.ca (M.K.); Nicolas.Galanis@USherbrooke.ca (N.G.)

* Author to whom correspondence should be addressed; E-Mail: Mikhail.V.Sorin@USherbrooke.ca;
Tel.: +1-819-821-8000 (ext. 62155); Fax: +1-819-821-7163.

Abstract: The Carnot factor *versus* enthalpy variation (heat) diagram has been used extensively for the second law analysis of heat transfer processes. With enthalpy variation (heat) as the abscissa and the Carnot factor as the ordinate the area between the curves representing the heat exchanging media on this diagram illustrates the exergy losses due to the transfer. It is also possible to draw the paths of working fluids in steady-state, steady-flow thermodynamic cycles on this diagram using the definition of "the equivalent temperature" as the ratio between the variations of enthalpy and entropy in an analyzed process. Despite the usefulness of this approach two important shortcomings should be emphasized. First, the approach is not applicable for the processes of expansion and compression particularly for the isenthalpic processes taking place in expansion valves. Second, from the point of view of rigorous thermodynamics, the proposed ratio gives the temperature dimension for the isobaric processes only. The present paper proposes to overcome these shortcomings by replacing the actual processes of expansion and compression by combinations of two thermodynamic paths: isentropic and isobaric. As a result the actual (not ideal) refrigeration and power cycles can be presented on equivalent temperature versus enthalpy variation diagrams. All the exergy losses, taking place in different equipments like pumps, turbines, compressors, expansion valves, condensers and evaporators are then clearly visualized. Moreover the exergies consumed and produced in each component of these cycles are also presented. The latter give the opportunity to also analyze the exergy efficiencies of the components. The proposed diagram is finally applied for the second law analysis of an ejector based refrigeration system.

1. Introduction

Utilisation of ejector refrigeration cycles powered by waste heat or solar energy is an important alternative to absorption machines such as LiBr-H$_2$O and H$_2$O-NH$_3$ [1,2]. Construction, installation and maintenance of such systems are relatively inexpensive compared to that of absorption machines. The temperature-entropy diagram is usually used to describe the behaviour of the ejector refrigeration cycles [3,4], however this diagram does not allow one to evaluate the irreversibilities, their distribution within the cycle, as well as the exergy efficiency of its components. The Carnot factor-enthalpy diagram has been used extensively for the second law analysis of heat transfer processes [5,6]. With enthalpy variation (heat) as the abscissa and the Carnot factor as the ordinate the area between the special curves, representing the heat exchanging media on this diagram, illustrates the exergy losses due to the transfer. The diagram has been applied for the thermodynamic analysis of individual heat exchangers [5] as well as for heat exchanger networks [6]. The introduction of the "equivalent temperature" allowed the sorption refrigeration cycles to be presented on this diagram [7]. Meanwhile the difficulties to present expansion and compression processes on the Carnot factor-enthalpy diagram limit its application to the ejector refrigeration cycles. The main objective of the present paper is to overcome this limitation by replacing the actual processes of expansion and compression by combinations of two thermodynamic paths: isobaric and isentropic. To explain this new approach the classical power cycle (Organic Rankine Cycle, ORC) and mechanical refrigeration cycle will be firstly presented on the Carnot factor-enthalpy diagram. Afterwards, following the work of Arbel *et al.* [8], the ejector refrigeration cycle will be presented as a superposition of the power and refrigeration cycles. It will allow presenting the ejector refrigeration cycle on the diagram. As a result the exergy losses as well as the exergies consumed and produced in each element of the ejector refrigeration cycle will be quantified and visualized on the diagram.

2. Equivalent Temperature

According to Prigogine [9] two thermodynamic processes are equivalent if the entropy production for each of them is the same. Following this definition, Bejan *et al.* [10] introduced the notion of "the equivalent temperature" as:

$$T_{eq} = \frac{\int_{in}^{out} T \cdot ds}{s_{out} - s_{in}} \qquad \text{with} \qquad \left(\frac{\dot{Q}_{VC}}{\dot{m}}\right)_{int, rev} = \int_{in}^{out} T \cdot ds \tag{1}$$

Given that the term (Tds) can be expressed as a function of enthalpy variation (dh):

$$Tds = dh - v \cdot dP \tag{2}$$

Equation (1) can be rewritten as:

$$T_{eq} = \frac{\left(h_{out} - h_{in}\right) - \int\limits_{in}^{out} v \cdot dP}{\left(s_{out} - s_{in}\right)} \tag{3}$$

Neveu and Mazet [7] defined the equivalent temperature (T_{eq}) simply by the ratio between the variations of enthalpy and entropy in an analyzed process:

$$T_{eq} = \frac{h_{out} - h_{in}}{s_{out} - s_{in}} = \left.\frac{\Delta h}{\Delta s}\right|_{p=Cst} \tag{4}$$

The later relation gave the opportunity to present a refrigeration cycle on the Carnot factor-enthalpy diagram. The Carnot factor was associated with (T_{eq}) by the following expression:

$$\Theta_{eq} = \left(1 - \frac{T_0}{T_{eq}}\right) \tag{5}$$

The comparison between Equations (3) and (4) shows that from the point of view of rigorous thermodynamics, the ratio (4) gives the correct equivalent temperature for isobaric processes only. This fact does not allow the application of the Carnot factor-enthalpy diagram [7] to compression and expansion processes. Moreover according to the definition (4) the equivalent temperature of a throttling process (dh = 0) is zero, as a result the exergy losses due to this process cannot be presented on such a diagram. Yet the application of ratio (4) is attractive because of its simplicity that already allowed the diagrammatic analysis of sorption refrigeration systems [5,6].

To keep the definition (4) for the analysis of ejector refrigeration cycles it is proposed to replace the adiabatic processes of expansion and compression by combinations of two thermodynamic paths: isentropic and isobaric. The value of T_{eq} for an isentropic process equals to (∞) which means that, according to (5), $\Theta_{eq} = 1$. For an isobaric process the values of T_{eq} and Θ_{eq} may be calculated by using the formulas (4) and (5) respectively. The next section will illustrate the application of this new approach to an ORC cycle.

3. Organic Rankine Cycle

The T-s diagram of the analyzed ORC is illustrated in Figure 1. The cycle was studied by Khennich and Galanis [11]. The working fluid is R152a. The cycle is used to recover the waste heat contained in a low temperature airstream rejected by an industrial process. This flow enters the evaporator at the temperature $T_{17} = 115\ °C$, the mass flow rate is $\dot{M}_s = 50\ kg/s$. The temperature of the cooling water at the condenser entry is $T_{15} = 10\ °C$ and the mass flow rate is $\dot{M}_p$. The working fluid receives heat at a relatively high pressure in the evaporator, is then expanded in a turbine, thereby producing useful work, and rejects heat at a low pressure in the condenser. It is then pumped to the evaporator. The isentropic efficiency of the pump is taken as $\eta_p = 1$. The isentropic efficiency of the turbine is equal to $\eta_T = 0.8$. The temperature difference between the external fluid inlet and the working fluid exit is taken as DT = 5 °C. The same DT is assumed for evaporator and condenser. The dimensionless value of the net power of the cycle α is obtained by dividing $(\dot{W}_T - \dot{W}_P)$ by the following reference power:

$$\dot{W}_{ref} = \dot{M}_s \cdot Cp_s \cdot (T_{17} - T_{15}) \cdot \left[1 - \frac{t_{15}}{t_{17}} \right].$$ The chosen value of α (=0.08) corresponds to a mass flow rate of

working fluid 4.177 kg/s. Finally, the evaporation pressure is considered equal to $P_{Ev} = 1000$ kPa. ($P_{Co} < P_{Ev} < P_{Sat}(T_3)$).

Figure 1. Temperature-entropy diagram of the ORC.
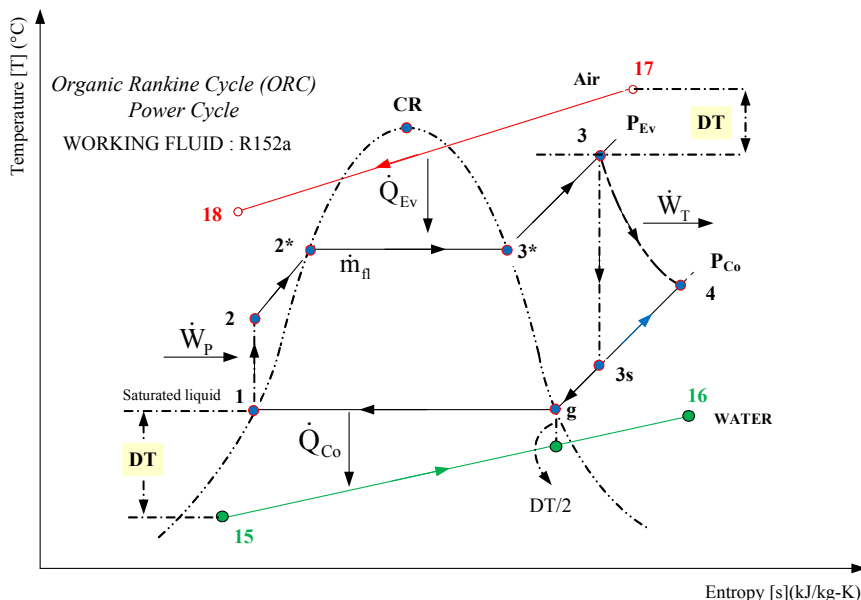
The adiabatic expansion path 3–4 is replaced by the combination of the isentropic path 3–3s and the isobaric 3s–4. The mathematical model of the cycle was solved by using the *EES* [12] code which includes the thermodynamic properties of R152a. The computational results, including Θ_{eq}, the corresponding enthalpy variations as well as the exergy losses and exergy efficiencies of each component of the cycle are presented in Figure 2.

Figure 2. Carnot factor based on the Eq. Temp., Enthalpy variations, Exergy losses and Exergy efficiencies of ORC components.

	Carnot factor based on Eq. Temperature Θ_{eq}			Energy		Ex. Losses	Ex. Efficiency
Power Cycle - ORC	Θ_{eq} $(1-T_0/T_{eq})$			Δh (kJ/kg)	ΔH **(kW)**	Ex_det (kJ/kg)	η_{Ex} (%)
TURBINE	Θ_{eq-33s}	1	Δh_{33s}	35.17	146.9	5.68	83.2
	Θ_{eq-43s}	0.1924	Δh_{43s}	7.03	29.4		
CONDENSER	Θ_{eq-41}	0.0381	Δh_{41}	369.46	1543.2	12.02	79.36
	$\Theta_{eq-1615}$	0.0056	Δh_{1615}	13.32	1543.2		
PUMP	Θ_{eq-21}	1	Δh_{21}	0.61	2.5	0.0	100,0
EVAPORATOR	$\Theta_{eq-1718}$	0.2379	Δh_{1718}	33.16	1658.0	47.29	79.79
	Θ_{eq-32}	0.1191	Δh_{32}	396.98	1658.1		

Flow rates of fluids in Power Cycle			Tot. Ex. Loss
			64.99 kJ/kg

Cycle (Working Fluid)	R152a	$\dot{m}_{fl}$	4.177 kg/s
Condenser (External Fluid)	Water	$\dot{M}_p$	115.854 kg/s
Evaporator (External Fluid)	Air	$\dot{M}_s$	50.0 kg/s

The Carnot factors corresponding to the isentropic expansion 3–3s and isentropic compression 1–2 equal 1, because the equivalent temperatures are infinitely large. The largest exergy losses take place at the evaporator, 197.53 kW (47.29 kJ/kg) and represent 72.77% of the total exergy destroyed 271.42 kW (64.99 kJ/kg) in the ORC system. However the exergy efficiency of the evaporator is relatively high, almost 80% which means that the further reduction of exergy losses may require an economically prohibitive increase in heat transfer area. The Θ_{eq} *vs.* ΔH results from Figure 2 are used to build the corresponding diagram presented in Figure 3.

Figure 3. Carnot factor based on Eq. Temp. *vs.* enthalpy variation for the ORC (not to scale).
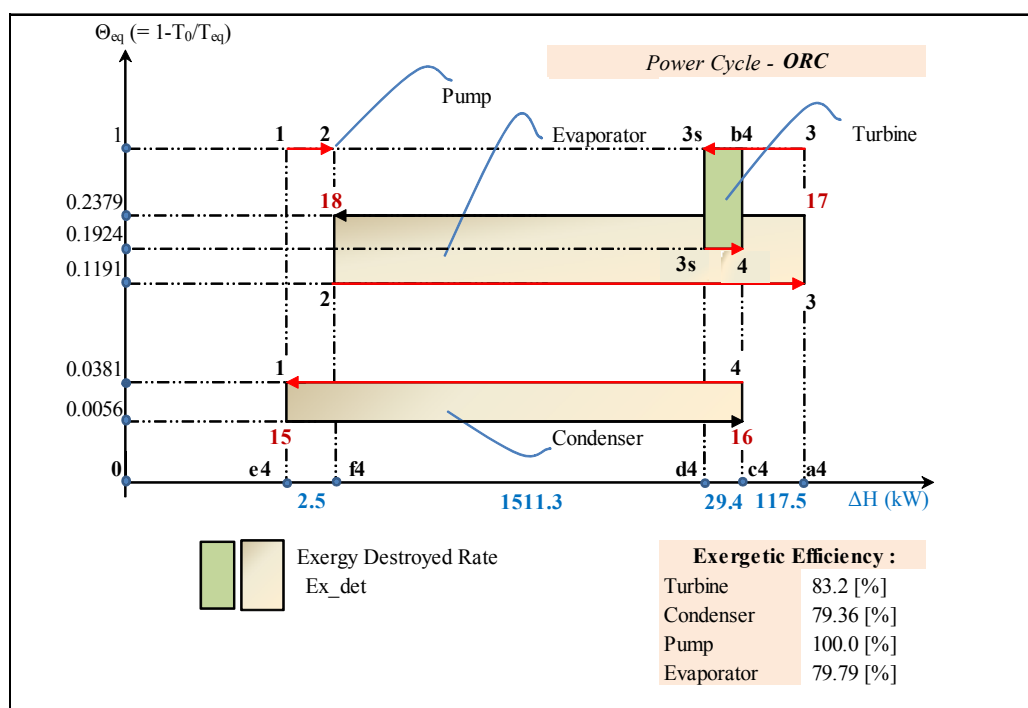
Although Figure 3 is not to scale, the information shown represents exactly the quantitative results of the analysis. For example, the exergy destruction in the turbine, in (kJ/kg), illustrated by the green rectangle in Figure 3 is equal to:

$$Ex\_det(TU) = \left(\Theta_{eq-33s} - \Theta_{eq-43s} \right) \cdot \frac{\Delta H_{43s}}{\dot{m}_{fl}}$$

$$= \frac{(1-0.1924) \cdot (29.4\,\mathrm{kW})}{(4.177\,\mathrm{kg/s})} = 5.68 \tag{6}$$

This result is identical to the corresponding value shown in Figure 2. The way to draw this diagram is to follow a particle of working fluid all along the cycle. It should be noted that the same point on T-s diagram is characterized by different equivalent temperatures depending on the process with which it is associated; it is therefore represented by multiple points on the same vertical line in the Θ_{eq}-ΔH diagram. For example point 3 on Figure 1 is the final state for the evaporation process 3–2 (Θ_{eq} = 0.1191) and the initial one for the expansion path 3–3s (Θ_{eq} = 1); as a result it is represented as two points on the same vertical line on Figure 3. Thus all the processes on the Θ_{eq}-ΔH diagram are presented by horizontal lines. The direction of the arrow corresponds to the direction of the working

flow. The isentropic expansion is presented by the line 3–3s at $\Theta_{eq} = 1$; the frictional (adiabatic) reheat of the turbine by line 3s–4 at $\Theta_{eq} = 0.1924$; the condensation by 4–1 at $\Theta_{eq} = 0.0381$; the isentropic pumping by 1–2 at $\Theta_{eq} = 1$ and the evaporation by 3–2 at $\Theta_{eq} = 0.1191$. The external fluids, hot gas and cooling water are presented by lines 17–18 and 16–15 respectively.

The closure of the energy balance of the cycle can be easily verified on this diagram. Indeed:

$$\dot{Q}_{Ev} + \dot{W}_P = \dot{Q}_{Co} + \dot{W}_T$$
$$(1658.1 + 2.5) = (1543.2 + (146.9 - 29.4)) \tag{7}$$

The results of the exergy analysis presented in Figure 2 are visually illustrated on the diagram of Figure 3. The exergy losses in each component of the ORC cycle are shown as surfaces and are the product of the enthalpy change ΔH in (kW) and the variation of the equivalent Carnot factor. The environmental temperature $T_0 = 283$ K (10 °C) is taken equal to the water temperature in the condenser. Moreover the diagram allows visualizing the exergy produced and expended in each element. Their ratio gives the value of exergy efficiency, Brodyansky *et al.* [13]. For example the area a4–3–b4–4–3s–d4 corresponds to the exergy produced by the turbine. It is composed of two useful effects: the shaft work from the turbine (the area a4–3–b4–c4) and the exergy of the frictional reheat (the area c4–4–3s–d4). The expended exergy is presented by the area a4–3–3s–d4 and corresponds to the exergy produced in the ideal isentropic turbine. The exergies produced in the evaporator and condenser are a4–3–2–f4 and c4–16–15–e4 respectively; the expanded exergies are a4–17–18–f4 and c4–4–1–e4 respectively.

4. Mechanical Refrigeration Cycle

The refrigeration mechanical vapor compression cycle is shown in Figure 4. The working fluid is R152a, the same as for the ORC. It enters the compressor at $T_1 = -10$ °C, ($T_1 = T_{4g} + 6$ °C) in the form of superheated steam (6 °C overheating at the outlet of evaporator). The isentropic compressor efficiency is $\eta_{Comp} = 0.85$. At the entrance of the condenser the fluid is in the form of superheated steam. It flows through the condenser by giving up heat to the external fluid (water). At the inlet of the expansion valve it is in the form of subcooled liquid (6 °C subcooling at the outlet of the condenser) $T_3 = 20$ °C, ($T_3 = T_{3f} - 6$ °C). It undergoes a pressure drop in the valve reaching the evaporation pressure at its outlet. Emerging from the valve, the fluid enters the evaporator as a liquid-vapor mixture. As it passes through the evaporator, it absorbs heat from the air, which enters at a temperature of 0 °C. The fluid finally leaves the evaporator in the form of superheated steam to be admitted into the compressor. The inlet temperature of the external fluid (water) in the condenser is 10 °C; a mass flow rate = 4 kg/s. The temperature difference between the refrigerant and the external fluid in the condenser and evaporator is DT = 10 °C. Refrigerant mass flow rate is = 0.15 kg/s. The flow regime is permanent and variations of the kinetic and potential energy are neglected. The throttling process 3–4 is replaced by the combination of the isentropic expansion path 3–3s and the isobaric-isothermal path 4–3s.

Similar to the ORC cycle the computational results, including Θ_{eq}, the corresponding enthalpy variations as well as the exergy losses and exergy efficiencies of each component of the refrigeration cycle are presented in Figure 5.

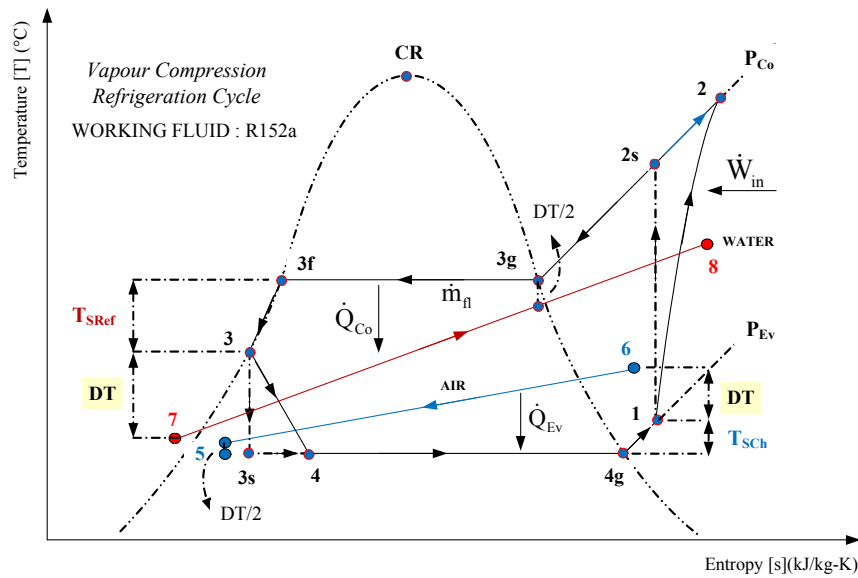**Figure 4.** Temperature-entropy diagram of the vapor compression cycle.

Figure 5. Carnot factor based on Eq. Temp., Enthalpy variations, Exergy losses and Exergy efficiencies of the Vapor compression cycle.

	Carnot factor based on Eq. Temperature Θ_{eq}			Energy	Ex. Losses	Ex. Efficiency
Vapour Compression Refrigeration Cycle	Θ_{eq}		Δh	ΔH	Ex_det	η_{Ex}
	$(1-T_0/T_{eq})$		(kJ/kg)	(kW)	(kJ/kg)	(%)
COMPRESSOR	$\Theta_{eq\text{-}2s1}$ = 1	Δh_{2s1} = 49.52		7.4	7.63	86.9
	$\Theta_{eq\text{-}22s}$ = 0.1269	Δh_{22s} = 8.74		1.3		
CONDENSER	$\Theta_{eq\text{-}23}$ = 0.0579	Δh_{23} = 324.93		48.7	17.17	8.8
	$\Theta_{eq\text{-}87}$ = 0.0051	Δh_{87} = 12.18		48.7		
EXPANSION VALVE	$\Theta_{eq\text{-}33s}$ = 1	Δh_{33s} = 4.47		0.7	4.92	0.0
	$\Theta_{eq\text{-}43s}$ = (-)0.1011	Δh_{43s} = 4.47		0.7		
EVAPORATOR	$\Theta_{eq\text{-}14}$ = (-)0.1008	Δh_{14} = 266.67		40.0	11.39	26.4
	$\Theta_{eq\text{-}65}$ = (-)0.0581	Δh_{65} = 11.06		40.0		

Flow rates of fluids in Refrigeration Cycle

Tot. Ex. Loss
41.11 kJ/kg

|			
Cycle (Working Fluid)	R152a	$\dot{m}_{fl}$	0.15 kg/s
Condenser (External Fluid)	Water	$\dot{m}_{Co}$	4.00 kg/s
Evaporator (External Fluid)	Air	$\dot{m}_{Ev}$	3.62 kg/s

Unlike the results for the ORC, Figure 5 illustrates that the biggest exergy losses take place in the heat exchangers of the refrigerating cycle. In the condenser, this translates into 41.77% of the total exergy destroyed in this cycle. The evaporator follows with 27.71% of the total exergy losses of the cycle. All exergy expended in the valve is destroyed by the irreversibility, thus its exergy efficiency is nil.

The Θ_{eq}-ΔH diagram of the cycle is presented on Figure 6. The isentropic compression is presented by the line 1–2s at Θ_{eq} = 1; the frictional (adiabatic) reheat of the compressor by line 2s–2 at Θ_{eq} = 0.1269; the condensation by 2–3 at Θ_{eq} = 0.0579; the isentropic expansion path by 3–3s at Θ_{eq} = 1; the isobaric-isothermal path by 3s–4 at Θ_{eq} = −0.1011 and the evaporation by 4–1 at Θ_{eq} = −0.1008. The external fluids, air and cooling water are presented by lines 6–5 and 7–8 respectively. Again the closure of the energy balance of the cycle can be easily verified on this diagram:

$$\dot{Q}_{Ev} + \dot{W}_{in} = \dot{Q}_{Co}$$
$$\left(40.0 + \left(7.4 + 1.3\right)\right) = \left(48.7\right) \tag{8}$$

Figure 6. Carnot factor based on Eq. Temp. *vs.* enthalpy variation for the vapor compression cycle (not to scale).
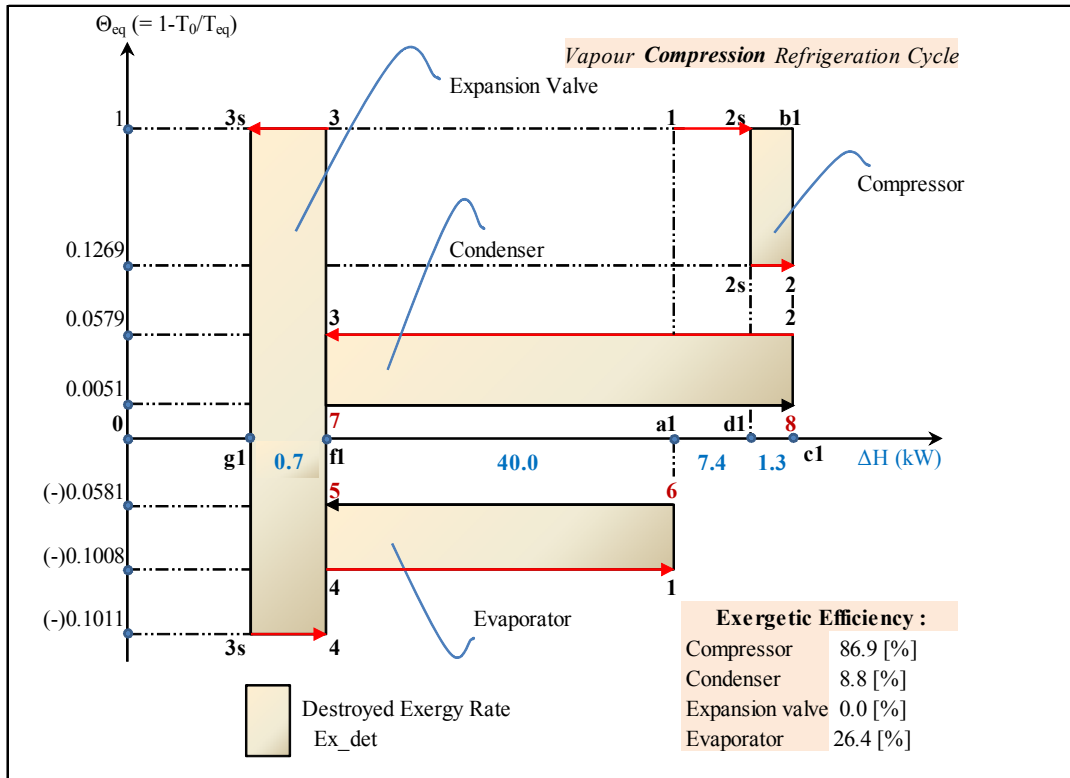
The diagram reveals the nature of exergy losses in the throttling valve. Indeed they are presented as a summation of two areas: the first (f1–3–3s–g1–f1) corresponds to the lost potential to produce shaft work due to the expansion, the second (f1–g1–3s–4–f1) illustrates the exergy lost due to the reduced refrigeration capacity in the evaporator.

The exergy produced by the compressor is presented by the area a1–1–2s–2s–2–c1. It is the sum of two components: the minimum shaft work to drive the isentropic compression (the area a1–1–2s–d1) and the exergy of the frictional reheat (the area d1–2s–2–c1). The expended exergy is presented by the area a1–1–b1–c1 and corresponds to the shaft work required to drive the real adiabatic compressor. The interpretation of the areas corresponding to exergies produced and expanded in heat exchangers are similar to the ORC case.

5. Ejector Refrigeration System

The ejector refrigeration cycle driven by solar energy is illustrated in Figure 7. The cycle has been studied under the condition of minimizing the total thermal conductance (UA_t) of the three heat exchangers (generator, condenser and evaporator). The corresponding optimum value of pressure at the generator is $P_{Ge,opt}$ = 3000 kPa resulting in a minimum total thermal conductance of $UA_{t,min}$ = 10.65 kW/K. The refrigerant used is R152a. External fluids at the generator, condenser and

evaporator are respectively: XcelTherm500, water and the anti-freezing fluid MEG 45% (monoethylene glycol 45%) as a coolant at low temperature. The refrigeration capacity has been set to a value of 10 kW. The minimum temperature difference in the heat exchangers is DT = 5 °C. The temperature of the fluid entering the generator is $T_{Ge,in}$ = 105 °C, the temperature of the cooling water entering the condenser is $T_{Co,in}$ = 10 °C and the temperature of the refrigeration fluid entering the evaporator is $T_{Ev,in}$ = 0 °C.

Figure 7. The ejector refrigeration cycle driven by solar energy.
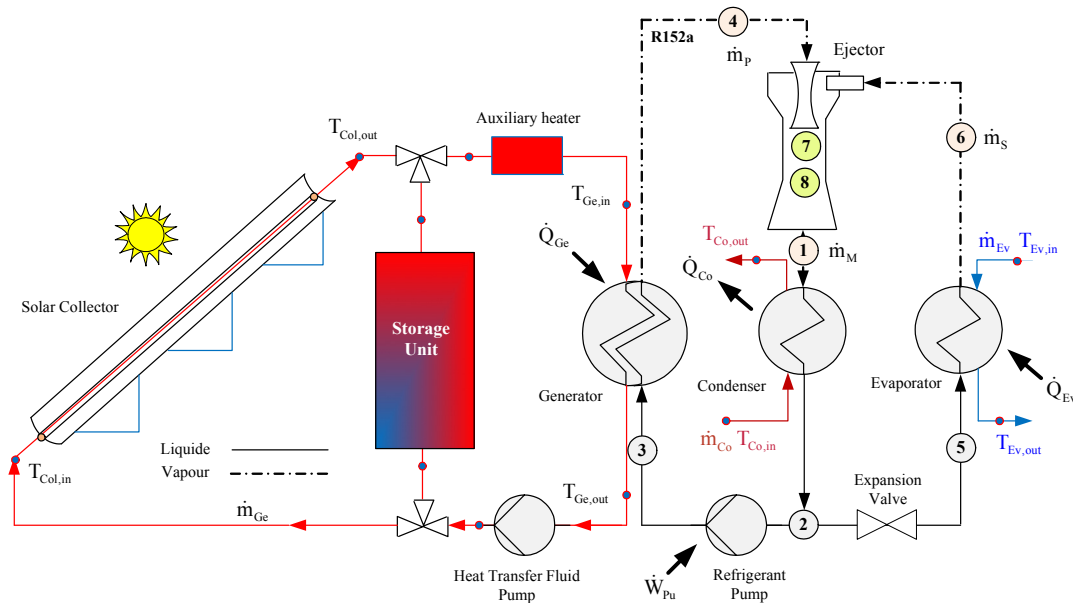
Figure 8 illustrates the four sections of an ejector: nozzle, suction chamber, mixing chamber and diffuser. The computational model used in the present study is based on the hypothesis of constant area of mixing chamber Dahmani *et al.* [3].

Figure 8. Four sections of a one phase ejector.

Figure 9 shows a temperature-entropy diagram of the processes taking place in the system presented on Figure 7 and the ejector on Figure 8. According to Dahmani *et al.* [3] the high pressure vapor at 4 expands isentropically in a converging–diverging nozzle to a very low pressure 7p and aspirates the saturated vapor from 6. The later expands to a pressure 7s, the same as at 7p. These two low pressure

streams mix irreversibly in a constant area chamber emerging at state 8. Finally this mixture is decelerated isentropically to state 1 in a diffuser.
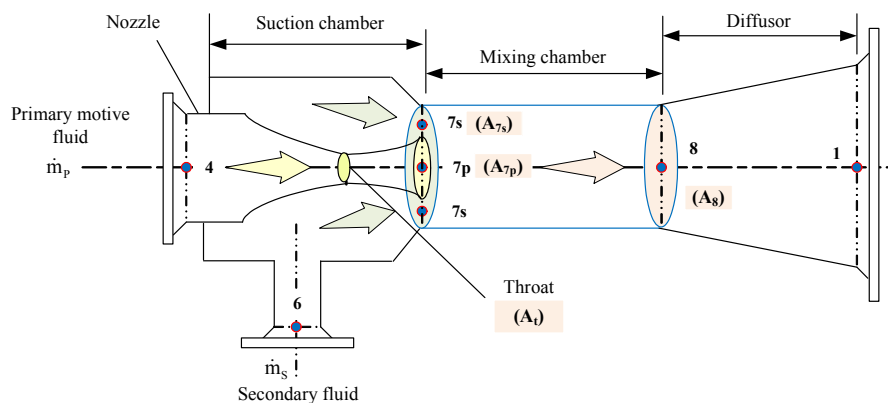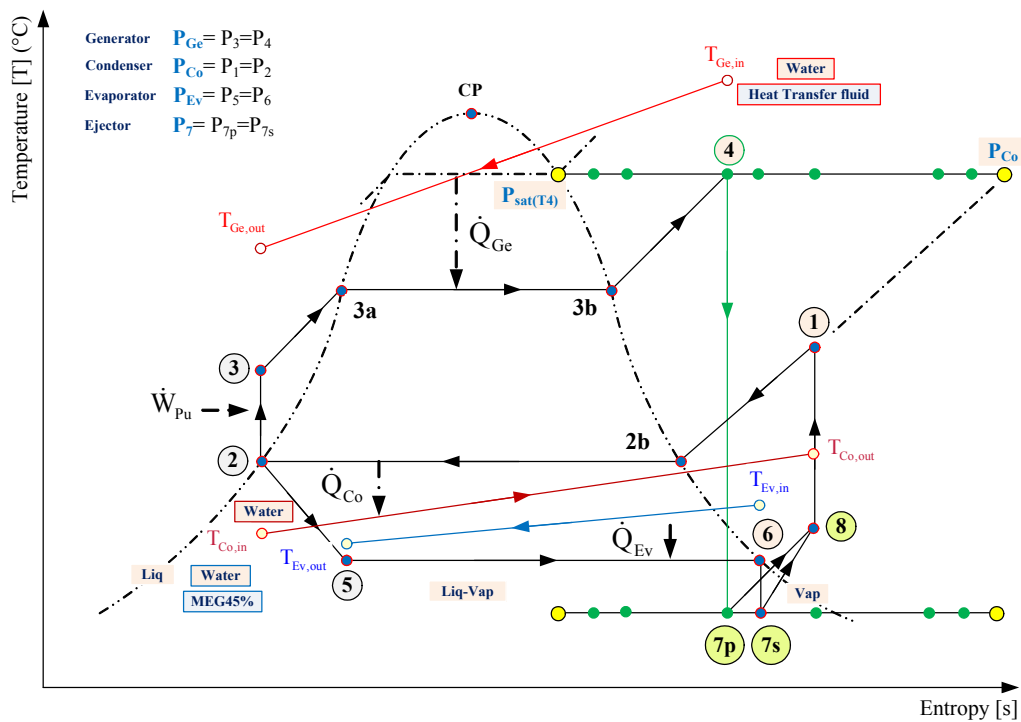
Figure 9. Temperature-Entropy diagram of the ejector refrigeration cycle.

The states of the refrigerant at all points of Figures 7 and 8 are calculated according to the procedure described by Dahmani *et al.* [3] using the following inputs: R152a, $\dot{m}_p = 0.040896$ kg / s $\dot{m}_s = 0.036090$ kg / s , (XcelTherm500, $T_{Ge,in} = 105$ °C), (Water, $T_{Co,in} = 10$ °C), (MEG45%, $T_{Ev,in} = 0$ °C), DT = 5 °C, $\dot{Q}_{Ev} = 10$ kW . This procedure considers that the acceleration of the primary and secondary fluids from 4 to 7p and from 6 to 7s respectively as well as the deceleration of the mixture from 8 to 1 are reversible and adiabatic (see Figure 9). On the other hand the mixing process which occurs between planes 7 and 8 is adiabatic but irreversible resulting in a significant entropy increase (see Figure 9) and exergy destruction. We thus obtain the values of the pressure, the temperature, *etc.* at all the states shown in Figures 7 and 8. In particular we obtain the entropy increase associated with the irreversible mixing process which takes place between planes 7 (where the two streams have the same pressure, $P_{7p} = P_{7s} = 128.4$ kPa, but different velocities and entropies) and 8 (where the flow is fully mixed). Thus, $s_4 = s_{7p} = 2.050$ kJ/(kg·K), $s_6 = s_{7s} = 2.131$ kJ/(kg·K) and $s_8 = s_1 = 2.160$ kJ/(kg·K). We are also able to calculate the rate of exergy destruction associated with this irreversible mixing process. It should be noted that the rate of exergy destruction for the entire ejector is the same as that of the mixing process since the expansion of the two fluids and the deceleration of the mixture in the diffuser are considered to be reversible.

Following the work of Arbel *et al.* [8], the ejector refrigeration cycle can be presented as a superposition of the power (2–3–4–7p–8–1) and refrigeration (2–5–6–7s–8–1) sub-cycles. By using the isentropic and isobaric paths between points (4, 1) and (6, 1) these two sub-cycles are presented separately on Figure 10. The power cycle is named Upper Cycle (UC) and refrigeration cycle Lower Cycle (LC).

Figure 10. Splitting of the ejector refrigeration cycle into two sub-cycles: Upper Cycle (UC) and Lower Cycle (LC).
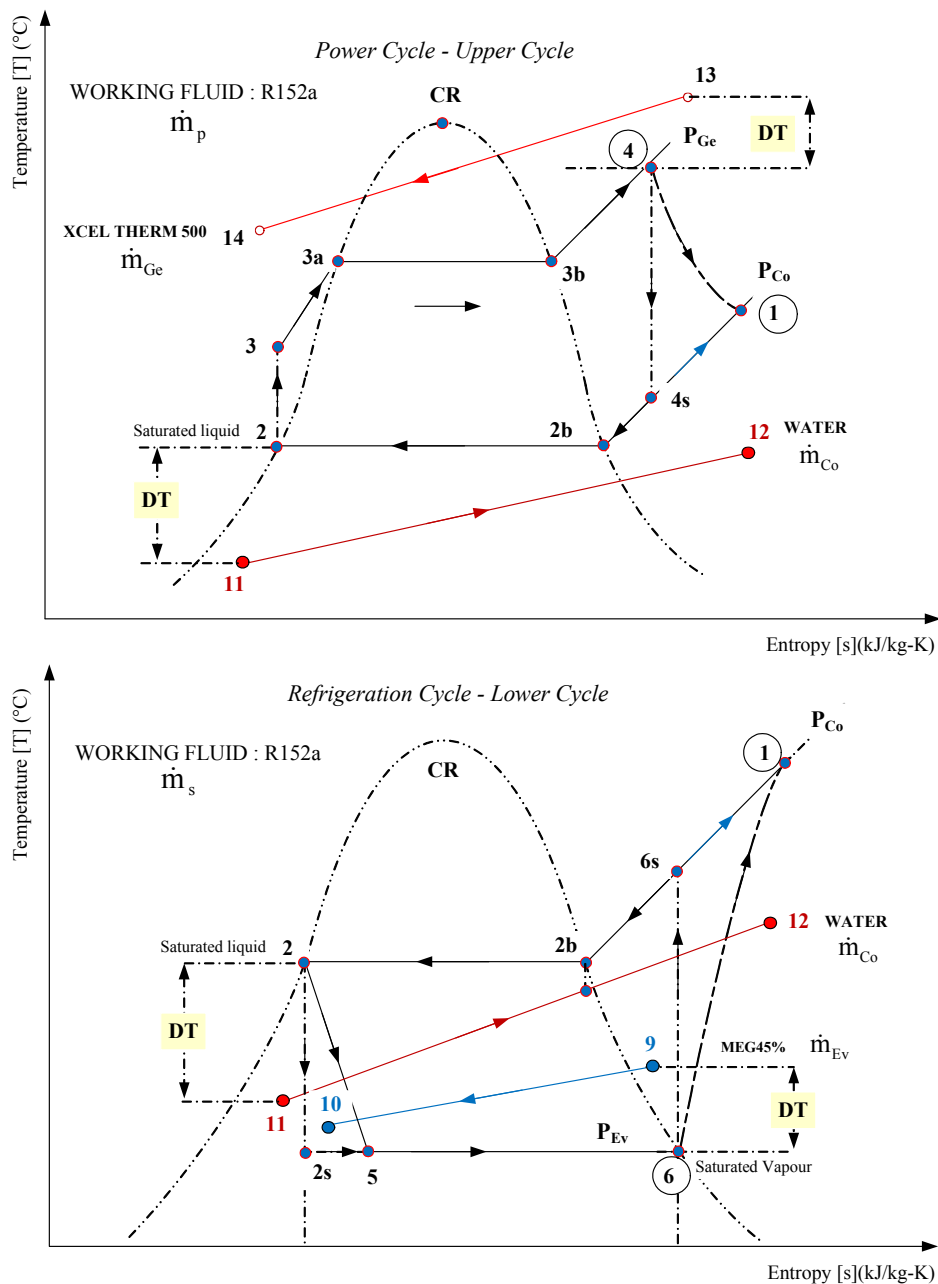
The power sub-cycle or Upper Cycle (UC) shown in Figure 10 is drawn using the intensive properties (temperature, pressure, specific entropy) of states 1, 2, 3 and 4 calculated by the Dahmani *et al*. [3] model for the cycle of Figure 9. It shows that the primary or motive fluid enters the ejector at state 4 and exits at state 1 with a considerable entropy increase caused by the irreversible phenomena taking place in the ejector. Similarly, the refrigeration sub-cycle or Lower Cycle (LC) of Figure 10 drawn with the intensive properties of states 1, 2, 5 and 6 (calculated by the model for the cycle of Figure 9) shows the corresponding entropy increase for the secondary or entrained fluid which enters the ejector at state 6 and exits at state 1. It should be noted that the two sub-cycles have the same intensive properties at states 1 and 2. The mass flow rates for the upper and lower sub-cycles are equal to primary and secondary mass flow rates of the ejector respectively.

The computational results, including Θ_{eq}, the corresponding enthalpy variations as well as the exergy losses and exergy efficiencies of each component of the two sub-cycles are presented in Figure 11.

Figure 11. Carnot factor based on Eq. Temp., Enthalpy variations, Exergy losses and Exergy efficiencies of Upper (UC) and Lower (LC) sub-cycles.

| *Ejector Power Cycle [UPPER Cycle]*		Carnot factor based on Eq. Temperature Θ_{eq}		Energy	Ex. Losses	Ex. Efficiency
		Θ_{eq}	Δh	ΔH	Ex_det	η_{Ex}
		$(1-T_0/T_{eq})$	(kJ/kg)	(kW)	(kJ/kg)	(%)
EJECTOR TURBINE-UC	Θ_{eq-44s}	1	Δh_{44s} 59.41	2.43	31.08	46.81
	Θ_{eq-14s}	0.0304	Δh_{14s} 32.06	1.31		
CONDENSER	Θ_{eq-12}	0.0187	Δh_{12} 308.08	12.60	3.01	93.97
	$\Theta_{eq-1211}$	0.0047	Δh_{1211} 5.90	12.60		
PUMP	Θ_{eq-32}	1	Δh_{32} 2.77	0.11	0.00	100.0
GENERATOR	$\Theta_{eq-1314}$	0.2311	Δh_{1314} 49.66	13.61	15.46	94.26
	Θ_{eq-43}	0.1847	Δh_{43} 332.7	13.61		

Flow rates of fluids in Power Cycle

Tot. Ex. Loss: 49.55 kJ/kg

Cycle (Working Fluid)	R152a	$\dot{m}_p$	0.040896 kg/s
Condenser (External Fluid)	Water	$\dot{m}_{Co}$	2.135 kg/s
Generator (External Fluid)	Xcel Therm 500	$\dot{m}_{Ge}$	0.274 kg/s

Ejector Refrigeration Cycle [LOWER Cycle]		Carnot factor based on Eq. Temperature Θ_{eq}		Energy	Ex. Losses	Ex. Efficiency
		Θ_{eq}	Δh	ΔH	Ex_det	η_{Ex}
		$(1-T_0/T_{eq})$	(kJ/kg)	(kW)	(kJ/kg)	(%)
EJECTOR COMPRESSOR-LC	Θ_{eq-6s6}	1	Δh_{6s6} 22.35	0.81	8.20	73.56
	Θ_{eq-16s}	0.0529	Δh_{16s} 8.65	0.31		
CONDENSER	Θ_{eq-12}	0.0187	Δh_{12} 308.08	11.12	2.64	94.71
	$\Theta_{eq-1211}$	0.0047	Δh_{1211} 5.21	11.12		
EXPANSION VALVE	Θ_{eq-22s}	1	Δh_{22s} 1.46	0.053	1.54	0.00
	Θ_{eq-52s}	(-)0.0559	Δh_{52s} 1.46	0.053		
EVAPORATOR	Θ_{eq-65}	(-)0.0559	Δh_{65} 277.08	10.0	4.03	93.57
	Θ_{eq-910}	(-)0.0414	Δh_{910} 8.35	10.0		

Flow rates of fluids in Refrigeration Cycle

Tot. Ex. Loss: 16.41 kJ/kg

Cycle (Working Fluid)	R152a	$\dot{m}_s$	0.036090 kg/s
Condenser (External Fluid)	Water	$\dot{m}_{Co}$	2.135 kg/s
Evaporator (External Fluid)	MEG45%	$\dot{m}_{Ev}$	1.198 kg/s

The irreversibility of the phenomena occurring in the entire ejector (see Figure 9) is equal to the sum of those occurring in the turbine of the Upper Cycle and the compressor of the Lower Cycle between states 4–1 and 6–1 respectively.

The Θ_{eq}-ΔH diagrams of the two sub-cycles are presented on Figure 12. For the UC the isentropic expansion of the motive stream is presented by the line 4–4s at $\Theta_{eq} = 1$; the frictional (adiabatic) reheat by line 4s–1 at $\Theta_{eq} = 0.0304$. For the LC the isentropic compression is presented by the line 6–6s at $\Theta_{eq} = 1$ whereas the frictional (adiabatic) reheat of the compressor is by line 6s–1 at $\Theta_{eq} = 0.0529$. The presentations of the processes in heat transfer equipment are similar to the diagrams on Figures 3 and 6.

Figure 12. Carnot factor based on Eq. Temp. *vs.* enthalpy variation for the Upper (UC) and Lower (LC) sub-cycles (not to scale).
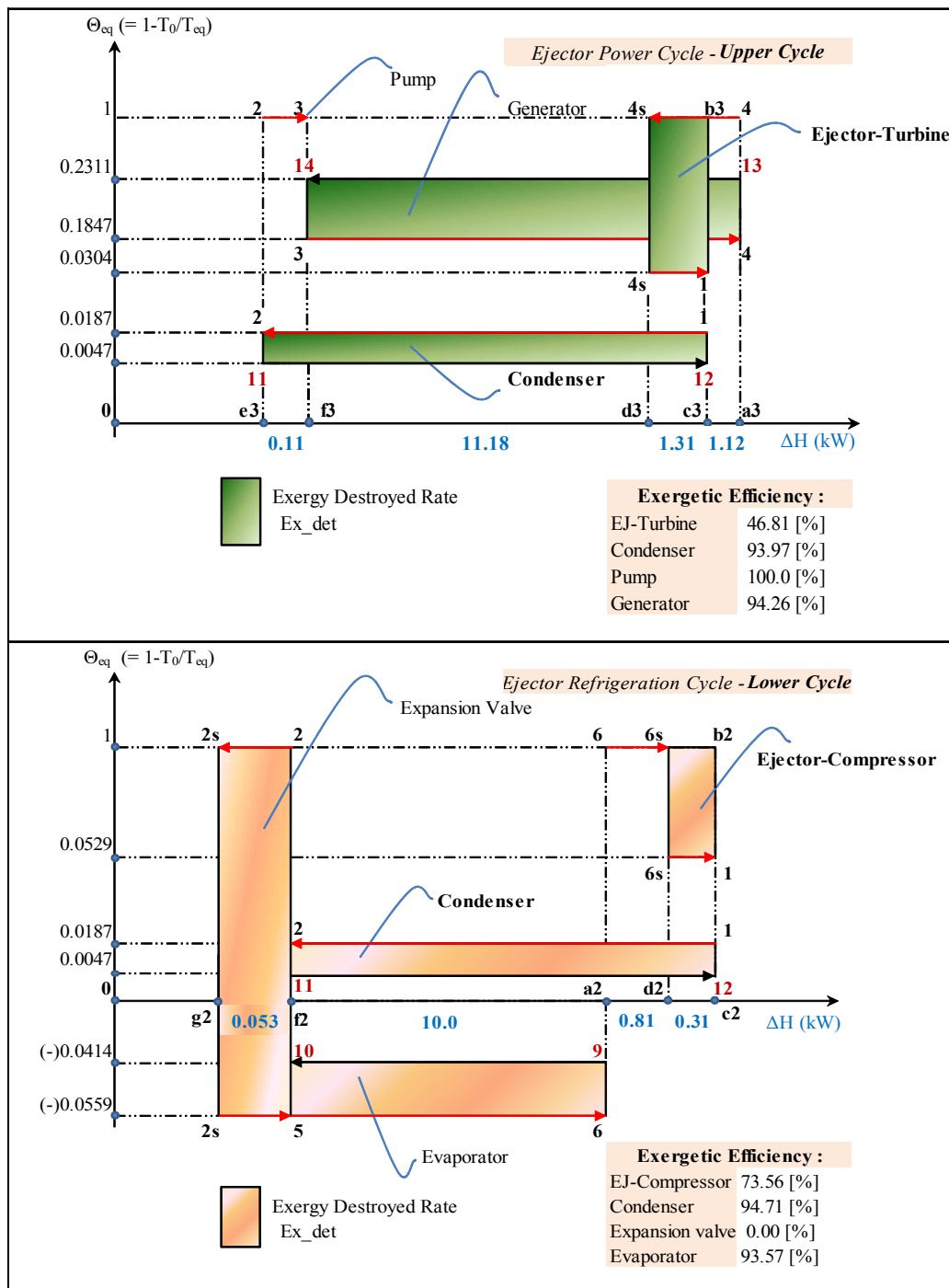
Again, even though Figure 12 is not to scale, the information shown represents exactly the quantitative results of the analysis. For example, the exergy destruction, in (kJ/kg), in the expansion valve is equal to:

$$Ex\_det(EVal) = \left(\Theta_{eq-22s} - \Theta_{eq-52s}\right) \cdot \frac{\Delta H_{52s}}{\dot{m}_s}$$

$$= \frac{(1 - (-0.0559) \cdot (0.053\,kW)}{(0.036090\,kg/s)} = 1.55 \tag{9}$$

The difference between this result and the corresponding value in Figure 11 is (0.01) kJ/kg (*i.e.*, less than 1%) and is due to rounding of errors.

Given that the ejector and the condenser are the pieces of equipment which connect the two sub-cycles, UC and LC, the exergy losses in (kW) calculated separately in these two components will therefore be added.

$$
\begin{aligned}
\dot{Ex}_{det(Ejector)} &= \dot{Ex}_{det(EJ-TU)} + \dot{Ex}_{det(EJ-CO)} \\
&= \Delta H_{14s} \cdot \left(1 - \Theta_{eq-14s}\right) + \Delta H_{16s} \cdot \left(1 - \Theta_{eq-16s}\right) \\
&= 1.564
\end{aligned}
\tag{10}
$$

$$
\begin{aligned}
\dot{Ex}_{det(Condenser)} &= \left(\left(\Delta H_{12}\right)_{UC} + \left(\Delta H_{12}\right)_{LC}\right) \cdot \left(\Theta_{eq-12} - \Theta_{eq-1211}\right) \\
&= 0.3321
\end{aligned}
\tag{11}
$$

Figure 13 is the zooming of the useful exergy produced (the left diagram) and the exergy expended (the right diagram) in the ejector taken from Figure 12.

Figure 13. The areas representing exergy produced and the exergy expended in the ejector (not to scale).
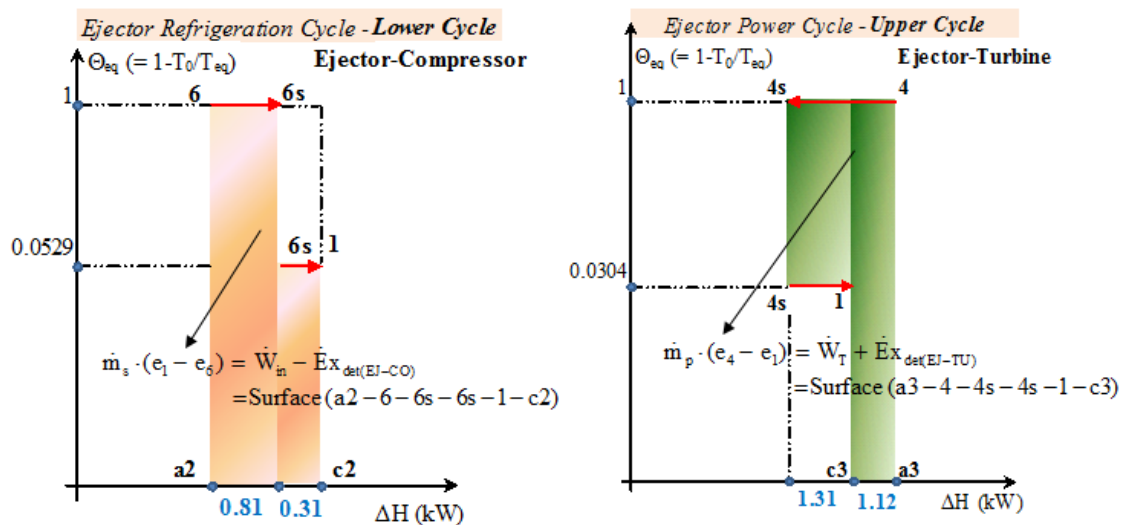
Based on Figure 13 the exergy efficiency in (%) is defined as:

$$
\begin{aligned}
\eta_{ex}^{ejector} &= \frac{\dot{W}_{in} - \dot{Ex}_{det(EJ-CO)}}{\dot{W}_{T} + \dot{Ex}_{det(EJ-TU)}} = \frac{\Delta H_{6s6} + \Delta H_{16s} \cdot \Theta_{eq-16s}}{\Delta H_{44s} - \Delta H_{14s} \cdot \Theta_{eq-14s}} \\
&= \frac{0.81 + (0.31) \cdot (0.0529)}{2.43 - (1.31) \cdot (0.0304)} = 34.57
\end{aligned}
\tag{12}
$$

This value is relatively low and emphasises the necessity to improve the thermodynamic efficiency of the ejector in the ejector refrigeration cycle.

6. Conclusions

- A special Carnot factor-enthalpy diagram based on "the equivalent temperature" has been proposed to analyse the exergy performance of ejector refrigeration cycles.

- The exergy losses as well as the exergies consumed and produced in each component of the ejector refrigeration cycle are qualitatively visualized on the diagram.
- The diagram pinpoints the low exergy efficiency of the ejector inside the ejector refrigeration cycle.

Acknowledgments

Author Contributions

Mohammed Khennich: Principal Investigator; Mikhail Sorin: Proposed the main idea of the paper; provided guidance and technical assistance; Nicolas Galanis: Provided technical and writing assistance.

Nomenclature

A	Area	m^2
DT	Temperature difference between working fluid and external fluid	°C
e	Specific flow exergy	kJ/kg
Eq. Temp.	Equivalent Temperature	
$\dot{Ex}_{det}$	Exergy destruction rate	kW
$\dot{E}'$	Exergy rate (Inlet)	kW
$\dot{E}''$	Exergy rate (Outlet)	kW
GWP	Global warming potential, relative to CO_2	
h	Specific enthalpy	kJ/kg
$\dot{m}_{fl}$	Mass flowrate of working fluid	kg/s
$\dot{M}_p, \dot{M}_s$	Mass flowrate of sink and source	kg/s
ODP	Ozone depletion potential, relative to R11	
ORC	Organic Rankine Cycle	
P	Pressure	kPa, MPa
$\dot{Q}$	Heat transfer rate	kW
s	Specific entropy	kJ/kg-K
T, Temp, t	Temperature, (t) is in K	°C, K
UA	Thermal conductance	kW/K
$\dot{W}$	Power input or output	kW
ΔH	Enthalpy variation rate: $\Delta H = \dot{m} \, \Delta h$	kW

Greek symbols

α	Non-dimensional net power output
η	Efficiency
Δ	Difference
Θ	Carnot Factor, $\Theta = (1 - T_0/T)$

Subscripts

0	Dead state
1, 2…3*…	States of thermodynamic cycle
Co	Condenser, condensation
CO, comp	Compressor, compression
CR	Critical
det	Destruction, destroyed
Ej	Ejector
Ev	Evaporator, evaporation
Eq, eq	Equivalent
ex	exergetic
fl	Fluid
g	Saturated vapor
Ge	Generator
in	Inlet, Input
is	Isentropic
LC	Lower Cycle
min	Minimal, minimum
opt	Optimal
out	Outlet, Output
p	Sink, primary
P	Pump
ref	reference
s	Source, secondary
SCH	Superheating
SRef	Subcooling
t	Total
T, TU	Turbine
UC	Upper Cycle
VC	Control volume
w	Specific work (inlet or outlet)

Conflicts of Interest

The authors declare no conflict of interest.

References

1. Jawahar, C.P.; Raja, B.; Saravanan, R. Thermodynamic studies on NH_3-H_2O absorption cooling system using pinch point approach. *Int. J. Refrig.* **2010**, *33*, 1377–1385.
2. Weber, C.; Berger, M.; Mehling, F.; Heinrich, A.; Nunez, T. Solar cooling with water-ammonia absorption chillers and concentrating solar collector—Operational experience. *Int. J. Refrig.* **2013**, doi: 10.1016/j.ijrefrig.2013.08.022.

3. Dahmani, A.; Galanis, N.; Aidoun, Z. Optimum design of ejector refrigeration systems with environmentally benign fluids. *Int. J. Therm. Sci.* **2011**, *50*, 1562–1572.

4. Alexis, G.K. Estimation of ejector's main cross sections in steam-ejector refrigeration system. *Appl. Therm. Eng.* **2004**, *24*, 2657–2663.

5. Ishida, M.; Kawamura, K. Energy and exergy analysis of a chemical process system with distributed parameters based on the enthalpy-direction factor diagram. *Ind. Eng. Chem. Process Des. Dev.* **1982**, *21*, 690–695.

6. Anantharaman, R.; Abbas, O.S.; Gundersen, T. Energy level composite curves—A new graphical methodology for the integration of energy intensive processes. *Appl. Therm. Eng.* **2006**, *26*, 1378–1384.

7. Neveu, P.; Mazet, N. Gibbs systems dynamics: A simple but powerful tool for process analysis, design and optimization. *ASME J. Adv. Energy Syst. Div.* **2002**, *42*, 477–483.

8. Arbel, A.; Shklyar, A.; Hershgal, D.; Barak, M.; Sokolov, M. Ejector Irreversibility characteristics. *J. Fluids Eng.-T. ASME* **2003**, *125*, 121–129.

9. Prigogine, I. *Introduction to Thermodynamics of Irreversible Processes*; John Wiley and Sons: New York, NY, USA, 1962.

10. Bejan, A.; Tsatsaronis, G.; Moran, M. *Thermal Design and Optimization*; John Wiley: New York, NY, USA, 1996; p. 542.

11. Khennich, M.; Galanis, N. Optimal design of ORC systems with a low-temperature heat source. *Entropy* **2012**, *14*, 370–389.

12. Klein, S.A. Engineering Equation Solver (EES), Academic Commercial V8.400. Available online: http://www.fchart.com/ees/ (accessed on 17 April 2014).

13. Brodyansky, V.M.; Sorin, M.; LeGoff, P. *The Efficiency of Industrial Processes: Exergy Analysis and Optimization*; Elsevier Science B. V.: Amsterdam, The Netherlands, 1994.